

Machine Learning-Based Digital Pre-Distortion Scheme for RoF Systems and Experimental 5G mm-waves Fiber-Wireless Implementation

Luiz A. M. Pereira^{ID}, Eduardo S. Lima^{ID}, Luciano L. Mendes^{ID}, Arismar Cerqueira S. Jr.^{ID}

National Institute of Telecommunications (Inatel)
510 João de Camargo Av., Santa Rita do Sapucaí-
MG, Brazil, 37540-000.

luiz.melo@inatel.br, elima@get.inatel.br, lucianol@inatel.br, arismar@inatel.br

Abstract— The advent of the 5th generation of mobile networks brought a large number of new use case and applications to be supported by the physical layer (PHY), which must be more flexible than all previous radio access networks (RAN). The concept of the centralized RAN (C-RAN) allows all the baseband processing to be performed in the central office, simplifying the network deployment and also allowing the operators to dynamically control the PHY according with the applications requirements. The radio-frequency (RF) signal generated by the C-RAN can be transported to the remote radio unit (RRU) by using a radio over fiber (RoF) system. In this paper, we propose two RoF approaches for composing the transport and access networks of the next-generation systems. The first investigation relies on the implementation of a machine learning-based digital pre-distortion (DPD), designed for RoF systems. In the second approach, we implement an RoF system and characterize the optical and electrical power levels aiming to reduce the RoF non-linear distortions. The overall link performance is evaluated by measuring the error vector magnitude (EVM_{RMS}) and 590 Mbit/s is achieved with EVM_{RMS} as low as 4.4% in a 10 m reach cell.

Index Terms— 5G NR, digital pre-distortion, fiber-wireless system, machine learning, radio over fiber.

I. INTRODUCTION

Mobile communication systems have been continuously evolving to support new communications features and enhance user experience. The introduction of the fifth-generation of mobile network (5G) has been remodeling the way that society uses telecommunication systems. The previous mobile networks, especially the third and fourth generations (3G and 4G) were mainly focused on redesigning the radio access network (RAN) in order to increase the system throughput. On the other hand, the 5G networks aim to bring innovative services and applications, favoring new vertical services, such as security improvement, agribusiness, vehicular communications, logistics, education, and health. These new applications and services impose contrasting and conflicting requirements to the physical layer (PHY), which must be flexible to be dynamically adapted for each scenario [1]–[4].

The optical/wireless convergence brings remarkable advantages, in particular, radio over fiber (RoF) technology is a key solution for transporting high-speed communications signals. The aforementioned

technology favors the centralized radio access network (C-RAN) design [5]. In such a system, the baseband processing is moved to a central office (CO), which allows sharing equipment and dynamic resource allocation leading to an expressive reduction in deployment costs [6]. The fronthaul link, which connects the CO and remote radio units (RRUs), might be implemented using wireless or optical technology. Typically, the optical link employs digital RoF (D-RoF) or analog RoF (A-RoF) [7]. In addition, signal transmission using RoF allows combining optical and wireless advantages, giving rise to the fiber-wireless (FiWi) system.

In an A-RoF implementation, the RF signal is applied to a Mach-Zehnder modulator (MZM) in order to modulate the optical carrier. This solution increases the transmission data rate compared to direct modulation. However, the MZM presents a non-linear behavior, which means that the ratio between the MZM output and input signals is a function of the radiofrequency (RF) input power. Typically, the non-linearities become more severe as the RF input power increases, producing in-band and out-of-band distortions. As a consequence, a limited RF power must be applied to the MZM input for minimizing the non-linearities in the MZM output. On the other hand, for specific applications, such as enhanced remote area communications (eRAC), high RF power is desirable to overcome the long optical link distance. In this case, a digital pre-distortion (DPD) technique must be employed to reduce the impacts of the non-linearities in the RoF signal [8].

The RoF system linearization might be performed either in the electrical or optical domain [9]–[13]. The DPD is the most prominent electrical-domain linearization technique. In RoF systems, DPD is commonly based on the non-linear Volterra model and Volterra derived models, such as memory and memoryless polynomial models [14]–[16]. Recently, machine learning (ML) solutions have attracted considerable attention in the context of signal processing techniques, since it is capable of performing complex computational tasks while requiring small computational power, making it an interesting tool for DPD implementation [17]–[19]. Therefore, ML algorithms can have a distinguish role in RoF systems employed in future FiWi communication.

The state-of-the-art on FiWi-based 5G architectures includes the coexistence investigation of 4G and 5G services [20], digital signal processing (DSP) for mitigating RoF degradation [21] and 5G signals distribution over passive optical networks (PON) [22]. Specifically, our research group has recently reported a non-standalone FiWi system for simultaneously transmitting 4G and 5G signals [23]. In the context of DSP-assisted 5G systems, we have used DSP for generating and pre-distort 5G signals, in the frequency range 1 (FR1) and frequency range 2 (FR2), in a multi-band FiWi system [24]. Moreover, we have presented a 5G multi-band system, which takes advantage of an active gigabit passive optical network (GPON) capillarity to distribute 5G signals.

The current paper is an extended version of our previous work [25]. It reports a validation of a ML-based technique for linearizing a RoF system. Additionally, we have implemented a multi-band FiWi system focused on the enhanced mobile broadband (eMBB) scenario for next-generation networks [26]. Our demonstration reports the following 5G applications: a 3.5-GHz 5G new radio (5G-NR) signal transport and transmission to cover outdoor eMBB scenario; a 26-GHz 5G-NR signal transport and transmission for covering indoor eMBB applications. The manuscript is structured in five sections. Section II introduces the ML-based DPD scheme proposed to mitigate the non-linearities introduced by the MZM and evaluates its performance. Section III describes the multi-band FiWi system, whereas Sections IV and V present the experimental results and conclusions, respectively.

II. A DIGITAL PRE-DISTORTION SCHEME BASED ON A MACHINE LEARNING TECHNIQUE

A. Methodology

RoF system can reduce the deployment and operational costs of mobile networks in remote areas. However, it is necessary to assure that the signals' characteristics at the RoF output, such as root mean square error vector magnitude (EVM_{RMS}) and out-of-band emission (OOBE), must be preserved. This means that the non-linearities introduced by the MZM must be compensated and the DPD is an efficient approach to achieve this goal. Conventional DPD schemes are very complex [15] and might require re-calibration over time. Therefore, we are proposing an ML linearization solution that is based on a linear regression technique. The employed artificial neural network (ANN) is composed of at least one input layer, one hidden layer, and one output layer, with non-linear activation functions.

The first architecture investigated in this paper is a multi-layer perceptron (MLP) ANN, which is the simplest ANN presented in the literature. In the MLP architecture, the neurons are densely connected. Each connection has its adjustable weights and bias. During the ANN training, the weights and bias parameters are adjusted accordingly to the backpropagation algorithm. In summary, the backpropagation training method uses a loss function to estimate the discrepancy between the ANN desirable training label and the ANN estimated output. During the training, the goal is to reduce the aforementioned discrepancy by updating the weights and bias set of parameters. The details of the architecture used to build the ML-based linearization scheme are presented below.

B. Artificial Neural Network Training

Fig. 1 illustrates the ANN training process. The desirable training labels consist of samples from a baseband orthogonal frequency division multiplexing (OFDM) signal (x_n), which are given by

$$x_n = \sum_{m=0}^{M-1} d_m e^{-j2\pi \frac{m}{M} n}, \quad (1)$$

where d_m represents the quadrature amplitude modulation (QAM) symbols that are mapped into M orthogonal subcarriers and $n \in \{0, 1, \dots, N-1\}$ is the time index. Next, the OFDM signal is applied to the RoF TX block, which is composed by a laser diode (LD) and an MZM. The MZM has a non-linear power response, which can be represented by the base-band memoryless polynomial model, defined as [17]

$$y_n = \sum_{k=0}^{K-1} h_k |x_n|^k x_n, \quad (2)$$

where h_k is the k th model coefficient, with $k = 0, 1, \dots, K-1$, in which K is the model non-linearity order. In this paper, we have used $K = 5$ to represent the MZM non-linearities. Since we are only interested in the MZM non-linearities, we have assumed that the single-mode fiber (SMF) and photodetector (PD) combined impulse response is $g_n = \delta_n$, leading to

$$z_n = y_n * g_n = y_n. \quad (3)$$

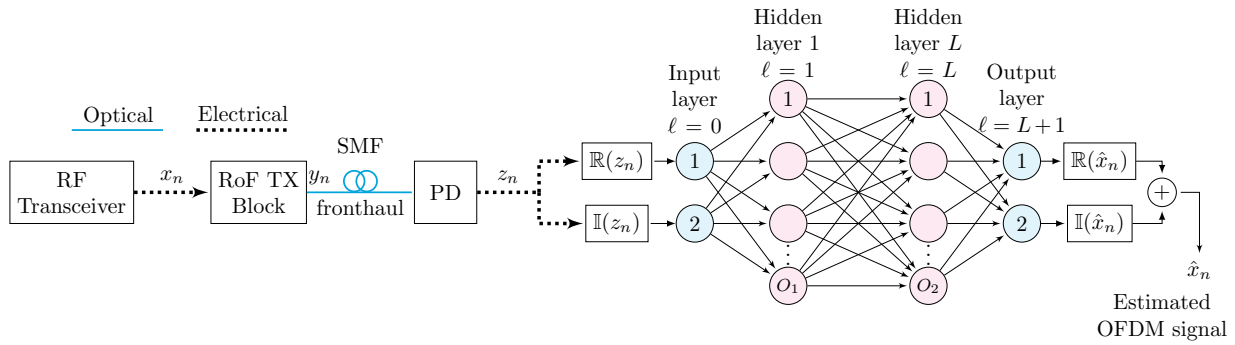


Fig. 1. MLP artificial neural network training process.

The PD output, z_n , is applied to train the ANN, whereas the training labels are the non-distorted OFDM signal, x_n . During the training, the ANN learns a function that approximates the RoF TX block post-inversion response, that will be used to pre-distort the OFDM signal.

The proposed ANN is composed of one input layer, two hidden layers, and one output layer. The number of neurons used in the ℓ th hidden layer, with $\ell \in \{1, 2, \dots, L\}$, is denoted by O_ℓ , with $O_1 = 64$ and $O_2 = 32$. The input and output layers have two neurons, i.e. $O_0 = O_{L+1} = 2$, being one for the real part and the other for the imaginary part of the OFDM signal. Table I summarizes the ANN hyperparameters that were tuned for optimizing the training process. The adaptive momentum (Adam) optimization algorithm was employed for training the ANN. It is well known that an ANN with a single hidden layer is capable of approximating any continuous function if enough data to train the ANN is provided. Considering the non-linear behavior of MZM, an elementary ANN employing non-linear activation functions can represent its non-linearities. Nevertheless, increasing the number of hidden layers also increases the non-linearities representation capability. Therefore, according to our empirical investigation and observations, a MLP ANN with two hidden layers and rectified linear unit (ReLU) activation function were enough to represent the non-linearities imposed by MZM. Furthermore, we have used a data set containing 20480 samples, which was split into a $N_{\text{TR}} = 14336$ training samples and $N_{\text{VAL}} = 6144$ validating samples. An early stop technique was employed to prevent overfitting in the ANN. We have set the patience hyperparameter to 100 and the training is concluded when the a mean-squared error (MSE) variation higher than 10^{-9} ($\Delta_{\text{min}} = 10^{-9}$) is not observed during 100 epochs.

TABLE I. MULTI-LAYER PERCEPTRON ANN HYPERPARAMETERS.

	Input Layer	Hidden Layer 1	Hidden Layer 2	Output Layer
Number of Neurons	2	64	32	2
Activation Function	-	ReLU	ReLU	Identity
Learning Rate		10 ⁻³		
Solver		Adam		
Loss Function		Mean-squared error		

C. Performance Analysis

After training the ANN, the obtained RoF TX block post-inversion estimation response are used to pre-distort the OFDM signal. Fig.2 depicts the block diagram of the RoF system, in which the ML-

based DPD block are placed between the RF transceiver and the RoF TX block. In this diagram, x_n , generated by (1), are applied to the ML-based DPD block, which has its output given by

$$v_n = \sum_{\ell=0}^{L+1} \phi(\mathbf{W}_\ell \times \mathbf{x}_\ell + \mathbf{b}_\ell), \quad (4)$$

where \mathbf{W} is a matrix of weights, \mathbf{x} is the input vector, \mathbf{b} is the biases vector and $\phi(\cdot)$ is the nonlinear activation function. It is important to highlight that in the first layer, \mathbf{x} is a vector produced by (1) containing all N samples and, in the sequential layers, \mathbf{x} is the output of the previous layer, since the layers are fully connected in the MLP architecture. The pre-distorted signal, v_n , is applied to the RoF TX block, which outputs y_n by applying (2) with v_n as input. Finally, the linearized version of the OFDM signal is given by (3). At the base station the linearized signal must be upconverted and amplified for the wireless transmission.

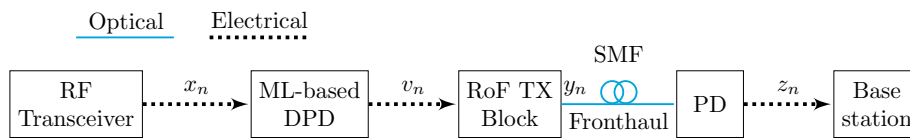


Fig. 2. Block diagram of the RoF system linearized using a ML DPD technique.

Fig. 3 presents the magnitude of the RF signal in the discrete time domain, which allows us verify the influence of the DPD scheme in the waveform. The DPD block applies the RoF TX block post-inversion response for pre-distorting the OFDM signal. As a result, the cascade response of the DPD block and the RoF TX block produces a linear response. Figs 3 (a) and (b) demonstrate that in the regions in which the non-linear RoF TX block response compress the signal, the DPD expands and vice versa. In other words, in the time-domain, the cascade response of the DPD block and the RoF TX block produces a signal as close as possible to x_n . It is well known that OFDM waveform presents a high peak-to-average power ratio (PAPR), which further aggravates the non-linear signal degradation. Once the linearization process produces a signal as close as possible to the original OFDM signal, the The PAPR of the linearized signal will similar to the original signal's PAPR.

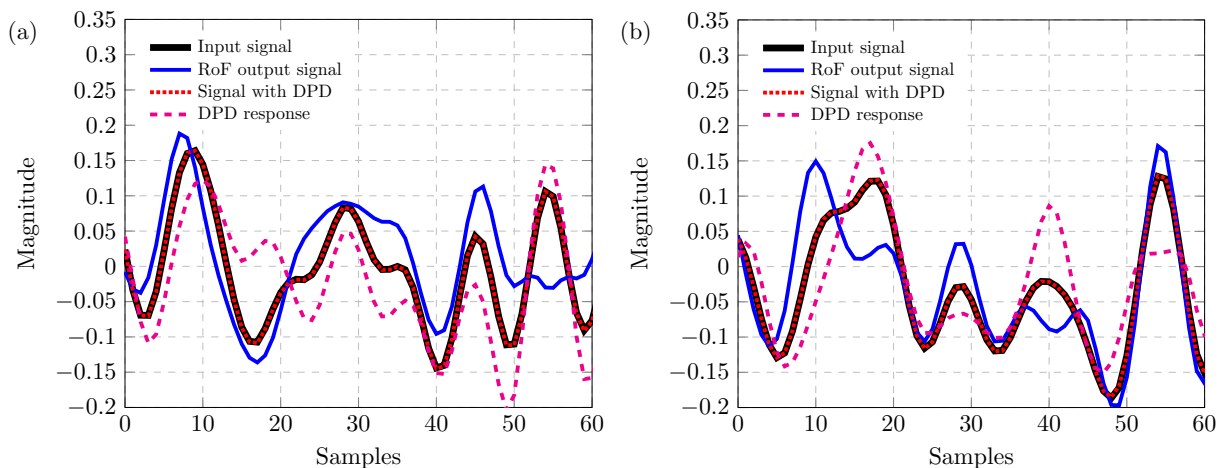


Fig. 3. OFDM Signal magnitude as a function of samples: (a) Real part; (b) Imaginary part.

We have also investigated the DPD effect on the OFDM signal in the frequency domain. Fig 4 (a) illustrates the normalized power spectrum density of the OFDM signal. We can note that our proposed ML-based DPD technique considerably reduces the OOB, resulting in an adjacent channel leakage ratio (ACLR) 10.5 dB below than the non-linearized signal. It is important to highlight that the DPD also reduces the in-band distortions resulting in the desired linear response. The DPD effect can also be seen in the signal constellation. Fig 4 (b) illustrates the constellation of the RoF output signal (blue circles) and the signal with DPD (red circles). The proposed technique has considerably reduced the symbols dispersion, leading to a EVM_{RMS} reduction from 6.35 to 0.92%.

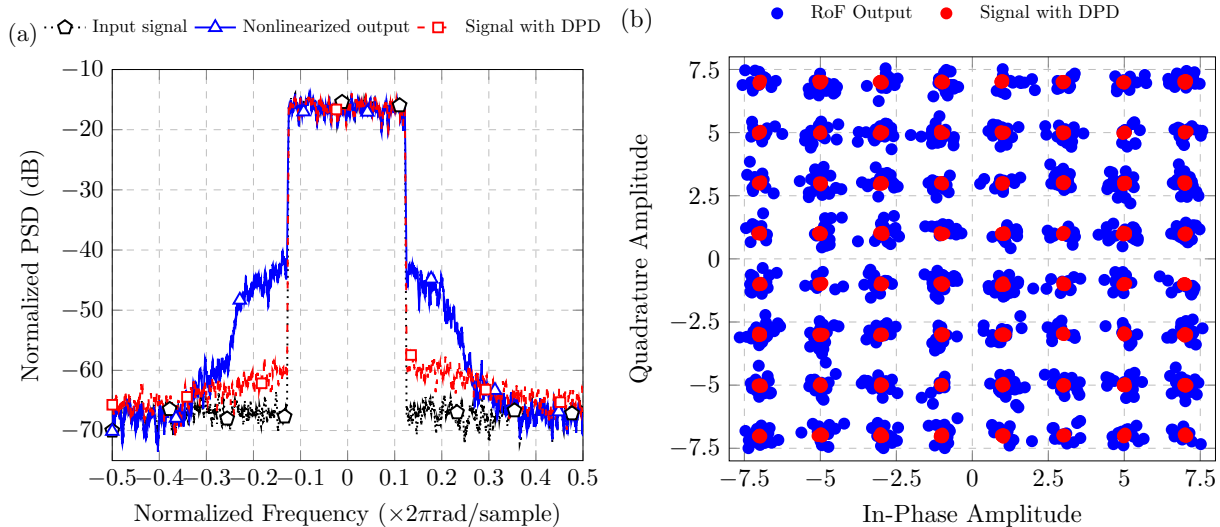


Fig. 4. Proposed DPD applied to an OFDM-16-QAM signal: (a) Normalized Power Spectrum Density; (b) Constellation.

III. 5G NR FIBER-WIRELESS SYSTEM

Fig. 5 describes the block diagram of our multi-band 5G-NR fiber-wireless system implementation. A LD from Golight generated a 10-dBm optical carrier at 1555 nm. Subsequently, a polarization controller (PC) has been employed to properly adjust and control the state of light polarization. A dual-drive Mach-Zehnder modulator (DD-MZM) has been used for simultaneously transmitting two distinct RF signals, namely: a 50-MHz bandwidth M -QAM 5G-NR signal at 3.5 GHz and a 100-MHz bandwidth M -QAM 5G-NR signal at 26 GHz, both in accordance to the 3rd Generation Partnership Project (3GPP) Release 15 [26]. The 5G signals were generated by Keysight arbitrary waveform generator (AWG) M8190A, using the Signal Studio software. Afterwards, the modulated optical carrier inset (i) propagated throughout a 12.5-km SMF fronthaul. The optical signal is then converted to electrical by an OPM + VOA and a photodetector (PD). The electrical signals are amplified by EA₁ and then split into two paths. Path (ii) goes through EA₂ and EA₄ to a transmitting antenna. Path (iii) goes through EA₃ and EA₅ to a receiving antenna. The received signals are then processed by a VSA.

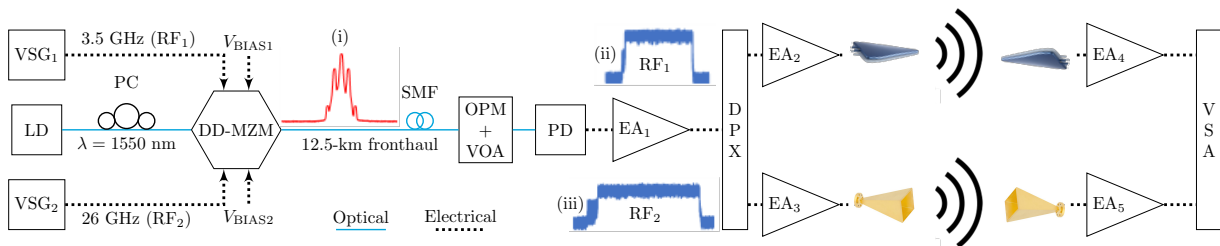


Fig. 5. FiWi system for the next-generation networks.

At the optical receiver, a variable optical attenuator (VOA) and an optical power monitor (OPM) ensured 2-dBm optical power at the PD input. The photodetector performed the optical-to-electrical conversion and launched the RF signals to a 24-dB gain broadband electrical amplification stage (EA_1). An electrical spectrum analyzer (ESA) has been used to measure the resultant electrical spectrum for both signals, which are presented in the insets (ii) and (iii). Afterward, a diplexer has separated the 5G-NR signals, which were individually transmitted employing proper antennas based on the frequency range.

The signal at 26 GHz has been amplified using (E_3) with 35-dB gain before feeding a 25-dBi gain horn antenna. On the other hand, a 20-dB gain amplifier (EA_2) has amplified the 3.5 GHz signal, which is subsequently transmitted by a 5-dBi gain log-periodic antenna, giving rise to 10-m wireless access implemented as a proof-of-concept. At the reception side, identical antennas have been used for receiving the 5G-NR signals. Sequentially, the received signals at 3.5 and 26 GHz have been individually amplified by (EA_4) and (EA_5) with 20-dB gain and 35-dB gain, respectively. Finally, a vector signal analyzer (VSA) has been used for evaluating the FiWi system performance based on EVM_{RMS} . Fig. 6 shows experimental setup photographs, including the transmitter and receiver sides.



Fig. 6. Photography of the experimental setup.

IV. EXPERIMENTAL RESULTS

This section presents an experimental investigation regarding the 5G-NR signals transport and transmission using our proposed FiWi System. Firstly, we have evaluated the transport RoF system performance, in terms of EVM_{RMS} , at two distinct setup stages, the photodetector input and the EA_1 output. Sequentially, we have investigated the wireless transmission system by transmitting the 3.5 and 26-GHz signals over a 10-m cell reach as a proof of concept.

Fig. 7 shows the EVM_{RMS} measurements as a function of the optical power at the photodetector input for the 3.5 and 26 GHz frequencies. In this analysis, we have used two modulation orders to investigate two distinct standardized 5G-NR bandwidths. Fig. 7 (a) shows the EVM_{RMS} performance for the 3.5-GHz 5G-NR signal modulated using 64/256-QAM and operating with 20 and 50-MHz bandwidths. One can note the EVM_{RMS} has kept below the 3GPP requirements from -16 to 2 dBm optical power

for the 64-QAM, whereas for the 256-QAM, the feasible EVM_{RMS} has varied from -12 to 2 dBm. It is worth mentioning the photodetector maximum optical input power has established the superior limiting power (2 dBm). Fig 7 (b) shows the EVM_{RMS} performance for the 26-GHz 5G-NR signal modulated with 16 and 64-QAM and operating with 50 and 100-MHz bandwidths. One can observe the higher operating frequency and bandwidths, in comparison to the 3.5GHz analysis, have required more optical power for achieving the 3GPP requirements, as expected. Finally, we can conclude the best RoF received optical power was about 0 dBm, considering both operating frequencies analyses.

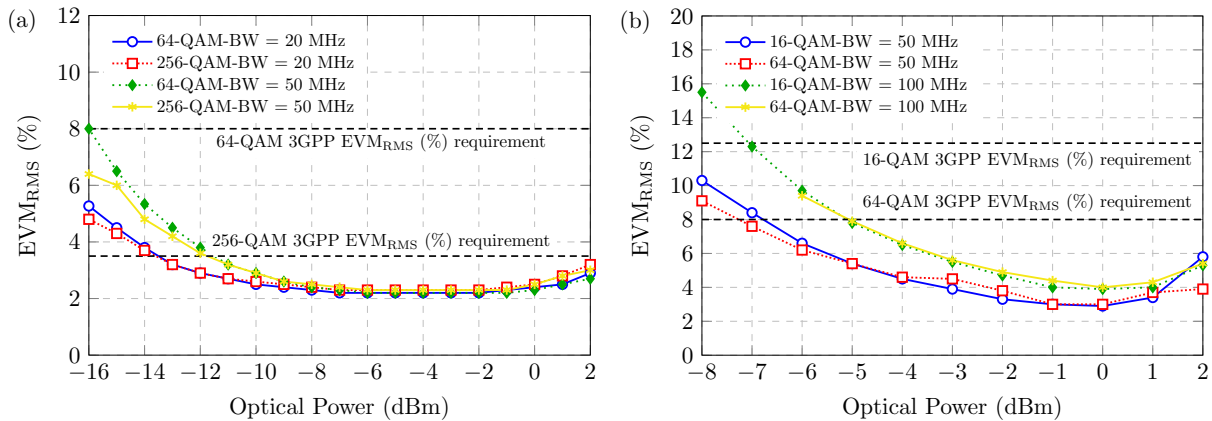


Fig. 7. EVM_{RMS} measurements as a function of the optical power at the photodetector input: (a) 3.5 GHz; (b) 26 GHz.

Our later analysis has consisted of varying the RF Mach-Zehnder modulator input power and measure the EVM_{RMS} at the EA_1 output, in order to obtain the best RF transmission power. Similarly to the optical power analysis, we have used the same modulation orders and bandwidths for this evaluation. Fig. 8 (a) and (b) report the EVM_{RMS} measure as a function of DD-MZM RF input power for the 3.5 and 26-GHz signals, respectively. The RF input power was varied from -26 to 6 dBm for the 3.5 GHz, whereas for the 26 GHz, the signal input powers varied from -8 to 6 dBm. One can note the EVM_{RMS} has increased for RF power above 1 dBm, decreasing the signal quality for both operating frequencies. This signal degradation occurs due to the DD-MZM non-linear response, which generates significant harmonics and inter-modulation products for powers higher than 1 dBm.

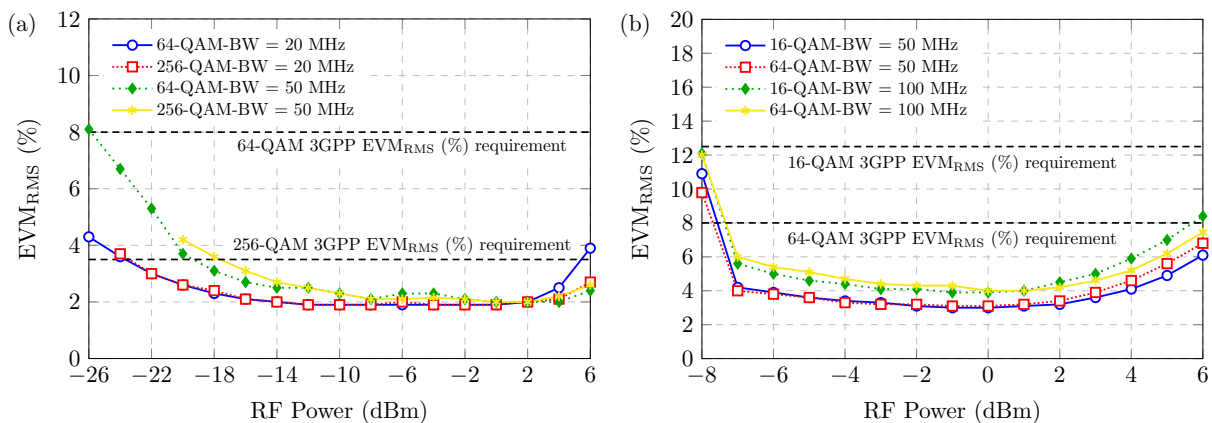


Fig. 8. EVM_{RMS} measurements as a function of RF power at EA_1 output: (a) 3.5 GHz; (b) 26 GHz.

One more time, the analyzed signals presented the same modulation orders and bandwidths from the previous results. We have implemented a 10-m reach FiWi system with 0 dBm received optical power at PD input and 0 dBm input RF power, which were the best configuration from our previous RoF performance evaluation. Fig. 9 shows the EVM_{RMS} measurements at the RX side for the 3.5 GHz and 26 GHz. The results show the received signals EVM_{RMS} measurements in the FR1 and FR2 bands, which has achieved EVM_{RMS} as low as 2.2 and 2.7% and 4.2 and 4.4%, respectively. For both operating frequencies, the FiWi system has been capable of recovering the signals with margins. These margins might be used to extend the link reach or to transmit signals with higher bandwidths. The joint transmission of signal with 50 MHz and 100 MHz bandwidths, has enabled attaining 590 Mbit/s throughput. Finally, our setup might be efficiently applied for composing the fronthaul and access networks for future communication systems.

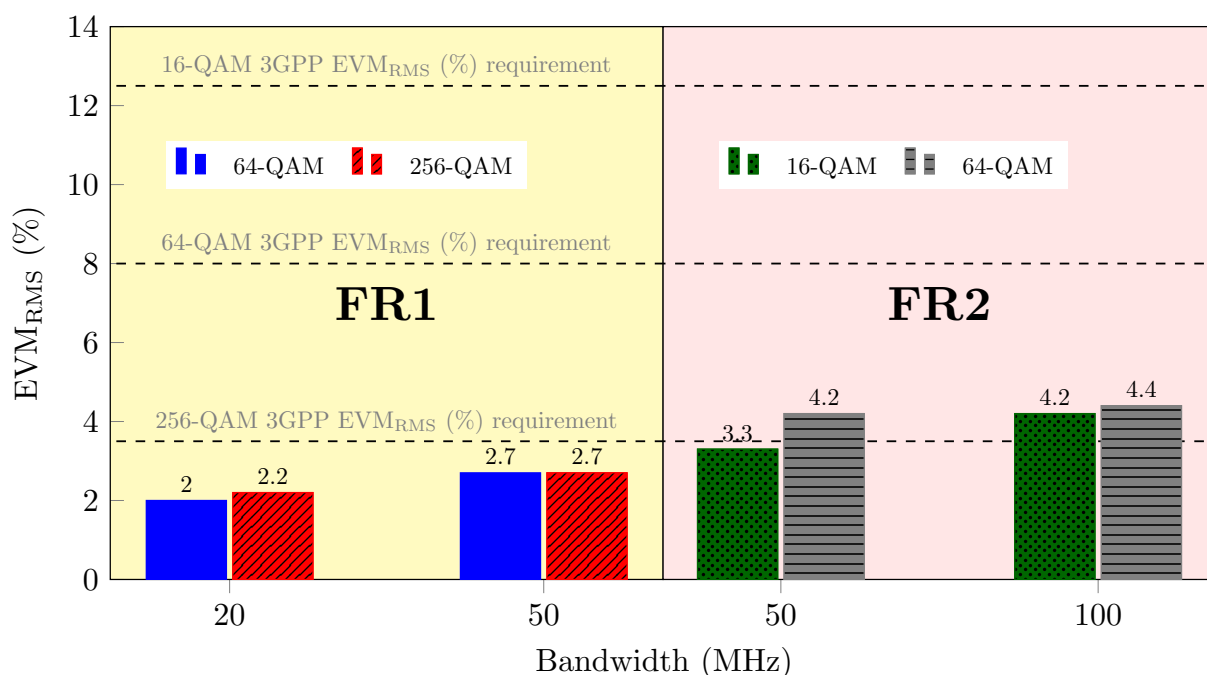


Fig. 9. 5G NR FiWi system EVM_{RMS} measurement as a function of bandwidth in the FR1 and FR2 bands.

Fig 10 illustrates the spectrum and constellation of the received 3.5 and 26 GHz signals after 10 m reach wireless transmission. In both frequency ranges, we have allocated half of the OFDM subcarriers for one user and the other half for a second user, following the orthogonal frequency division multiple access (OFDMA) operating principle. Fig.10 (a) illustrates the 50 MHz bandwidth received signal at 3.5 GHz, whereas Fig.10 (b) exhibit the 100 MHz bandwidth signal at 26 GHz. The assigned modulation orders were 64- and 256-QAM for the signal at 3.5 GHz, and 16- and 64-QAM for the signal at 26 GHz. The assigned modulation order depends on the user distance from the base stations (BS), i.e., the user located at BS proximity receives the signal with higher modulation order than that one at the cell border.

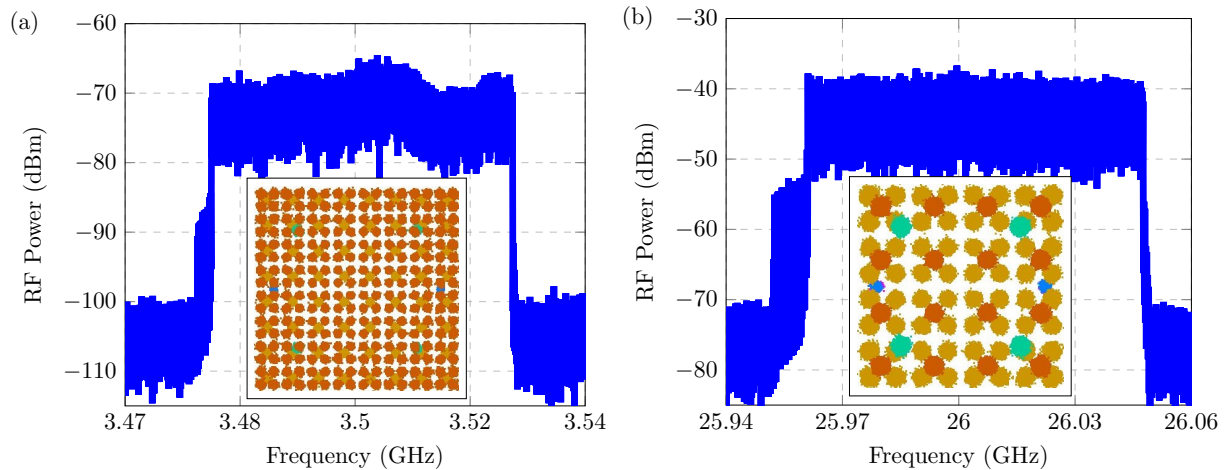


Fig. 10. Spectrum and constellation of the received signal after the wireless transmission: (a) 50-MHz bandwidth signal at 3.5 GHz; (b) 100-MHz bandwidth signal at 26 GHz.

V. CONCLUSIONS

This work reported a DPD technique based on a ML algorithm and the implementation of a multi-band FiWi system for the next-generation wireless networks. The proposed technique was applied to an OFDM signal and its performance was investigated in terms of EVM_{RMS} and ACLR. The proposed DPD scheme reduced 10.5 dB on the signal ACLR, while improving the EVM_{RMS} from 6.35 to 0.92%. This analysis demonstrated that ML algorithms can have a distinguish role in RoF systems employed in future FiWi communication.

We have also implemented an experimental multi-band FiWi system. In this second analysis, we were specially interested in the experimental validation of an C-RAN-based architecture for future FiWi systems. The results demonstrated our FiWi system as a potential solution for composing the transport and access network of the future communication systems. We reported an optical and electrical power characterization for the RoF transport network. Additionally, it was implemented a 10-m reach cell attaining 590 Mbit/s as a proof of concept. Futures works regard to join our two investigations, which means experimentally implement our proposed ML-based linearization technique in a multi-band 5G FiWi system.

ACKNOWLEDGMENTS

This work was partially supported by FAPESP Grant No. 20/05127-2, under SAMURAI project and Rede Nacional de Ensino e Pesquisa (RNP), with resources from the Ministério da Ciência, Tecnologia e Inovações e Comunicações (MCTIC), Grant No. 01245.020548/2021-07, under the 6G Mobile Communications Systems project of the Centro de Referência em Radiocomunicações (CRR) of the Instituto Nacional de Telecomunicações (Inatel), Brazil. Authors also thank the financial support from Conselho Nacional de Desenvolvimento Científico e Tecnológico (CNPq), Coordenação de Aperfeiçoamento de Pessoal de Nível Superior (CAPES), Financiadora de Estudos e Projetos (FINEP) and Fundação de Amparo à Pesquisa do Estado de Minas Gerais (FAPEMIG).

REFERENCES

- [1] M. Alsenwi, N. H. Tran, M. Bennis, A. K. Bairagi, and C. S. Hong, "eMBB-URLLC Resource Slicing: A Risk-Sensitive Approach," *IEEE Communications Letters*, vol. 23, no. 4, pp. 740–743, 2019.
- [2] G. P. Fettweis, "The Tactile Internet: Applications and Challenges," *IEEE Vehicular Technology Magazine*, vol. 9, no. 1, pp. 64–70, 2014.
- [3] I. Philbeck, "Connecting the Unconnected: Working Together to Achieve Connect 2020 Agenda Targets," in *Special session of the Broadband Commission and the World Economic Forum at Davos Annual Meeting*, 2017.
- [4] N. Xia, H.-H. Chen, and C.-S. Yang, "Radio Resource Management in Machine-to-Machine Communications—A Survey," *IEEE Communications Surveys Tutorials*, vol. 20, no. 1, pp. 791–828, 2018.
- [5] M. A. Habibi, M. Nasimi, B. Han, and H. D. Schotten, "A comprehensive Survey of RAN Architectures Toward 5G Mobile Communication System," *IEEE Access*, vol. 7, pp. 70 371–70 421, 2019.
- [6] V. A. Thomas, M. El-Hajjar, and L. Hanzo, "Performance Improvement and Cost Reduction Techniques for Radio over Fiber Communications," *IEEE Communications Surveys & Tutorials*, vol. 17, no. 2, pp. 627–670, 2015.
- [7] A. Udalcovs, M. Levantesi, P. Urban, D. A. Mello, R. Gaudino, O. Ozolins, and P. Monti, "Total Cost of Ownership of Digital vs. Analog Radio-Over-Fiber Architectures for 5G Fronthauling," *IEEE Access*, vol. 8, pp. 223 562–223 573, 2020.
- [8] J. Wang, C. Liu, M. Zhu, A. Yi, L. Cheng, and G.-K. Chang, "Investigation of Data-Dependent Channel Cross-Modulation in Multiband Radio-Over-Fiber Systems," *Journal of Lightwave Technology*, vol. 32, no. 10, pp. 1861–1871, 2014.
- [9] X. Zhang, "Broadband Linearization for 5G Fronthaul Transmission," *Frontiers of Optoelectronics*, vol. 11, no. 2, pp. 107–115, 2018.
- [10] T. Ismail, C.-P. Liu, J. E. Mitchell, and A. J. Seeds, "High-Dynamic-Range Wireless-Over-Fiber Link Using Feedforward Linearization," *Journal of Lightwave Technology*, vol. 25, no. 11, pp. 3274–3282, 2007.
- [11] S. Korotky and R. de Ridder, "Dual Parallel Modulation Schemes for Low-Distortion Analog Optical Transmission," *IEEE Journal on Selected Areas in Communications*, vol. 8, no. 7, pp. 1377–1381, 1990.
- [12] B. Masella, B. Hraimel, and X. Zhang, "Enhanced Spurious-Free Dynamic Range Using Mixed Polarization in Optical Single Sideband Mach-Zehnder Modulator," *Journal of Lightwave Technology*, vol. 27, no. 15, pp. 3034–3041, 2009.
- [13] G.-W. Lee and S.-K. Han, "Linear Dual Electroabsorption Modulator for Analog Optical Transmission," *Microwave and Optical Technology Letters*, vol. 22, no. 6, pp. 369–373, 1999.
- [14] M. Noweir, Q. Zhou, A. Kwan, R. Valivarathi, M. Helaoui, W. Tittel, and F. M. Ghannouchi, "Digitally Linearized Radio-Over Fiber Transmitter Architecture for Cloud Radio Access Network's Downlink," *IEEE Transactions on Microwave Theory and Techniques*, vol. 66, no. 7, pp. 3564–3574, 2018.
- [15] H. D. Rodrigues, T. C. Pimenta, R. A. A. de Souza, and L. L. Mendes, "Orthogonal Scalar Feedback Digital Pre-Distortion Linearization," *IEEE Transactions on Broadcasting*, vol. 64, no. 2, pp. 319–330, 2018.
- [16] A. Hekkala, M. Hiiuala, M. Lasanen, J. Perttu, L. C. Vieira, N. J. Gomes, and A. Nkansah, "Predistortion of Radio Over Fiber Links: Algorithms, Implementation, and Measurements," *IEEE Transactions on Circuits and Systems I: Regular Papers*, vol. 59, no. 3, pp. 664–672, 2012.
- [17] L. A. M. Pereira, L. L. Mendes, C. J. A. Bastos-Filho, and Arismar Cerqueira, S. Jr., "Linearization Schemes for Radio Over Fiber Systems Based on Machine Learning Algorithms," *IEEE Photonics Technology Letters*, vol. 34, no. 5, pp. 279–282, 2022.
- [18] M. U. Hadi, "Mitigation of Nonlinearities in Analog Radio over Fiber Links Using Machine Learning Approach," *ICT Express*, vol. 7, no. 2, pp. 253–258, 2021.
- [19] S. Liu, Y. M. Alfidhli, S. Shen, M. Xu, H. Tian, and G.-K. Chang, "A Novel ANN Equalizer to Mitigate Nonlinear Interference in Analog-RoF Mobile Fronthaul," *IEEE Photonics Technology Letters*, vol. 30, no. 19, pp. 1675–1678, 2018.
- [20] A. O. Mufutau, F. P. Guiomar, M. A. Fernandes, A. Lorences-Riesgo, A. Oliveira, and P. P. Monteiro, "Demonstration of a Hybrid Optical Fiber–Wireless 5G Fronthaul Coexisting With end-to-end 4G Networks," *IEEE/OSA Journal of Optical Communications and Networking*, vol. 12, no. 3, pp. 72–78, 2020.
- [21] H. Zeng, X. Liu, S. Megeed, A. Shen, and F. Effenberger, "Digital Signal Processing for High-Speed Fiber-Wireless Convergence [invited]," *IEEE/OSA Journal of Optical Communications and Networking*, vol. 11, no. 1, pp. A11–A19, 2019.
- [22] K. Kanta, A. Pagano, E. Ruggeri, M. Agus, I. Stratakos, R. Mercinelli, C. Vagionas, P. Toumasis, G. Kalfas, G. Giannoulis, *et al.*, "Analog Fiber-Wireless Downlink Transmission of IFoF/mmWave over In-Field Deployed Legacy PON Infrastructure for 5G Fronthauling," *IEEE/OSA Journal of Optical Communications and Networking*, vol. 12, no. 10, pp. D57–D65, 2020.

- [23] C. H. de Souza Lopes, E. S. Lima, L. A. M. Pereira, R. M. Borges, A. C. Ferreira, M. Abreu, W. D. Dias, D. H. Spadoti, L. L. Mendes, and A. Junior, "Non-Standalone 5G NR Fiber-Wireless System Using FSO and Fiber-Optics Fronthauls," *Journal of Lightwave Technology*, vol. 39, no. 2, pp. 406–417, 2021.
- [24] R. M. Borges, L. A. M. Pereira, H. R. D. Filgueiras, A. C. Ferreira, M. S. B. Cunha, E. R. Neto, D. H. Spadoti, L. L. Mendes, and Arismar Cerqueira S. Jr., "DSP-based flexible-waveform and multi-application 5G fiber-wireless system," *Journal of Lightwave Technology*, vol. 38, no. 3, pp. 642–653, 2020.
- [25] L. Pereira, E. Lima, and A. Cerqueira, "A Multi-band 5G-NR Fiber-wireless System for Next-generation Networks," in *2021 SBMO/IEEE MTT-S International Microwave and Optoelectronics Conference (IMOC)*, pp. 1–3, 2021.
- [26] 3GPP, "5G; NR; Overall description; Stage-2," *TS 38.300 version 15.3.1 Release 15*, 2018.